IEEE Access
Multidisciplinary | Rapid Review | Open Access Journal

Received May 26, 2020, accepted June 2, 2020, date of current version June 17, 2020.

Digital Object Identifier 10.1109/ACCESS.2020.3000671

Cramer-Rao Bounds of Localization Estimation for Integrated Radar and Communication System

TUANWEI TIAN[1], XIAOLIN DU[2], AND GUCHONG LI[1], (Student Member, IEEE)
[1]School of Information and Communication Engineering, University of Electronic Science and Technology of China, Chengdu 611731, China
[2]School of Computer and Control Engineering, Yantai University, Yantai 264005, China

Corresponding author: Xiaolin Du (duxiaolin168@vip.163.com)

This work was supported in part by the National Natural Science Foundation of China under Grant 61801415, and in part by the Shandong Provincial Natural Science Foundation, China, under Grant ZR2016FB22.

ABSTRACT Instead of only considering the radar estimation error in the traditional radar system (TRS), for the integrated radar and communication system (IRCS), we investigate the Cramer-Rao bound (CRB) of the localization estimation, which is influenced by both radar estimation error and communication transmission error. The functions of radar and communication are operated simultaneously by embedding the communication symbols into the multicarrier radar waveforms. Firstly, we derive the CRB of time/direction of arrival (TOA/DOA) estimation. To minimize the estimation error, we maximize the signal-to-interference-plus-noise ratio (SINR) of radar by iteratively optimizing the radar transmit and receive beamformers (with the constraint of available transmit power). Then, the CRB of localization estimation is derived using hybrid TOA/DOA measurement. The local CRBs from different IRCSs are fused according to the linear fusion rule at the fusion center (FC). Finally, numerical results demonstrate that the additional estimation errors for the IRCS are mainly determined by the channel conditions of communication and available transmit power; the estimation accuracy for both IRCS and TRS can be improved through the iterative transmit and receive beamforming (ITRB) technique.

INDEX TERMS Cramer-Rao bound, localization estimation, multicarrier waveform, beamforming, integrated radar and communication system.

I. INTRODUCTION

Radar and communication systems have been widely studied as two independent entities [1]. In general, target localization [2]–[4] is one of the main functions of the traditional radar system (TRS) whereas the traditional communication system is used to share information with other derives [5]. However, considering the increasing strain on limited spectral resources and the demand for hardware unification, it is necessary to integrate radar system with the communication system and solve the problems of the generalization and rational use of the system resources [6]–[8]. Two research directions of co-existence are developed and summarized as follows.

- *Spectral co-existence between radar and communication systems*. The achievable performance bounds of co-existence are derived in [9]. The successive interference cancellation (SIC) technique is adopted to handle the mutual interference caused by each other. For the sake of minimizing the interference caused by the co-frequency signal, the null-space projection (NSP) technique is adopted in [10]. The authors in [11] investigate the joint design problem of the radar waveform and the communication encoding matrix. The adopted design criterion is the maximization of the compound rate with the constraint of radar signal-to-interference-plus-noise ratio (SINR). The problems of transceiver design and power allocation are jointly solved in [12]. A system-level interference cancellation algorithm is proposed in [13] to deal with the situation where radar estimation is unreliable. The authors in [14], [15] analyze the problem of power minimization-based radar waveform design considering the existence of a communication signal on the same band. In [16], spectrum sharing based on co-design transmitted waveform is studied to minimize the effective interference from each

The associate editor coordinating the review of this manuscript and approving it for publication was Wei Liu.

other. The problems of power allocation and joint design between radar and communication systems are studied in [17], [18].

- *Dual-function radar and communication (DFRC) system that simultaneously operates the functions of radar and communication*. The main DFRC strategies include waveform diversity-based method [19], [20], time-modulated array method [21], amplitude modulation (AM) method [22], phase-shift keying (PSK) method [23]–[25] and quadrature amplitude modulation (QAM) method [26]. The waveform diversity-based method [19], [20] enables the communication function by exploiting waveform diversity while maintaining the performance of the radar. The authors in [21] introduce a time-modulated array method, which operates the radar function in the mainlobe and the communication function in the sidelobe. The AM method mentioned in [22] exploits two beamforming weight vectors with different sidelobe levels (SLLs) towards to communication receivers locating in the sidelobe region. Each sidelobe level is mapped to a unique communication symbol. In PSK-based strategy [23]–[25], information embedding is achieved by different phase to communication receivers. By exploiting sidelobe control and waveform diversity, the QAM strategy is proposed in [26]. Multiple communication receivers located in the sidelobe region can be supported by the proposed QAM-based technique.

Following [19]–[26], the functions of radar and communication can be realized by an integrated radar and communication system (IRCS). That is, we can simultaneously estimate the information of interest target and transmit the obtained information to other systems. For the TRS, Cramer-Rao bound (CRB) is a vital parameter to evaluate the estimation performance [27], [28]. The problem of direction of arrival (DOA) estimation is introduced in [29]–[35]. The authors in [36], [37] investigate the problem of two-dimensional (2-D) DOA estimation, and an extended study is presented in [38] wherein 2D direction-of departure (DOD), 2D-DOA, 2D receive polarization angle and 2D transmit polarization angle are estimated simultaneously. The stochastic CRB on joint DOD and DOA estimation is derived in [39] and the corresponding explicit closed-form expressions are given in [40]. Considering the impact of static phase errors at the transmitters and receivers, the authors in [41] derive the CRB of target localization by modeling the phase errors as random variables. The CRB of hybrid time of arrival (TOA) and DOA estimation is derived in [42]–[45].

However, only the radar estimation error is measured for the TRS. When we share the obtained position information of the target with other systems, the communication transmission error should also be considered because of the imperfect communication channel, communication receiver noise and so on. Therefore, for an IRCS, the CRB of localization estimation is a compound of the radar estimation error and communication transmission error. To the authors' best knowledge, the CRB of localization estimation for the IRCS is not yet available in the open literature. This is indeed the main topic of this paper. Summing up, the contributions of this work are the following.

- Different from the work in [22], where only transmit beamforming (TB) technique is adopted to realize both functions simultaneously, in this work, we propose an iterative transmit and receive beamforming (ITRB) technique for two purposes: 1) synthesize transmit beamformers with different SLLs (each SLL is mapped to a unique communication symbol), which enables information streams towards the FC while keeping the radar main beam at a desired magnitude; 2) obtain a higher radar SINR gain with the constraint of available transmit power.
- We derive the CRBs of the TOA/DOA estimation for the IRCS,[1] which are determined by the conditions of radar and communication channels simultaneously.
- We derive the CRB of localization estimation using hybrid TOA/DOA measurement. Combining local observations from different IRCSs, the fused CRB of localization estimation is derived at the fusion center (FC) by adopting linear fusion rule.
- Numerical results demonstrate that the additional estimation errors for the IRCS are mainly determined by the channel conditions of communication and available transmit power; the estimation accuracies can be improved through the iterative transmit and receive beamforming technique.

This paper is organized as follows. The signal model is introduced in Section II. In Section III, the CRBs of TOA and DOA estimation for the IRCS are derived. Section IV presents the CRB of localization estimation using hybrid TOA/DOA estimation and the local CRBs from different IRCSs are fused according to the linear fusion rule at the FC. Section V gives a numerical example, with conclusions drawn in Section VI.

Notations: Superscripts $(\boldsymbol{x})^T$ and $(\boldsymbol{x})^\dagger$ denote transpose and complex conjugate transpose of $\boldsymbol{x}$, respectively; $\mathbb{C}$ denotes the set complex number; $\mathbb{C}^N$ and $\mathbb{C}^{N\times N}$ denote the set of $N \times 1$ vectors and $N \times N$ matrices with complex entries, respectively; $E\{x\}$ denotes statistical expectation; $\boldsymbol{I}_N$ is the $N \times N$ identity matrix; $|\boldsymbol{X}|$ and $\|\boldsymbol{X}\|$ represent the modulus and norm of $\boldsymbol{X}$, respectively; $det\,(\boldsymbol{X})$ and $tr\,(\boldsymbol{X})$ indicate the determinant and trace of the matrix $\boldsymbol{X}$, respectively; $diag\{x_1, \ldots, x_n\}$ is the diagonal matrix with diagonal entries $x_1, \ldots, x_n$; $blkdiag\{\boldsymbol{X}_1, \ldots, \boldsymbol{X}_n\}$ is the block diagonal matrix with diagonal blocks $\boldsymbol{X}_1, \ldots, \boldsymbol{X}_n$; $vec\{\boldsymbol{x}_1, \ldots, \boldsymbol{x}_n\}$ is the vector obtained by stacking up $\boldsymbol{x}_1, \ldots, \boldsymbol{x}_n$.

II. SIGNAL MODEL

As depicted in Fig. 1, we consider a network consisting of J IRCSs wherein each IRCS equips with one integrated transmit array consisting of N_T antennas, one radar receive array consisting of $N_{R,r}$ antennas, and one (or more)

[1]The CRB in this paper is referred to the deterministic CRB.

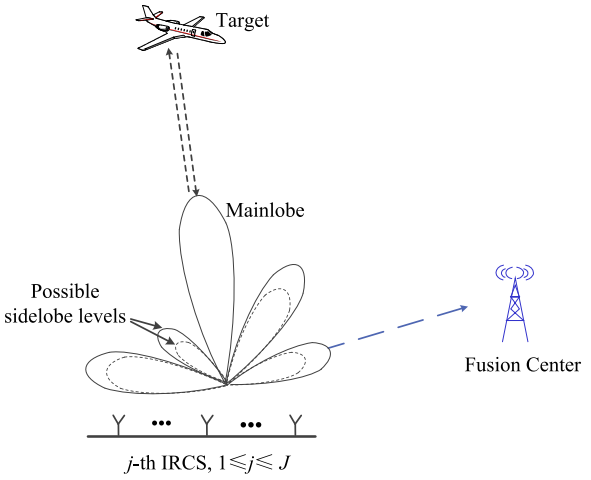

FIGURE 1. Each IRCS in the network detects the position of the target (x_T, y_T) and shares the position information with the FC.

communication receive array(s) consisting of $N_{R,c}$ antennas. Without loss of generality, we assume $N_{R,r} = N_{R,c} = N_R$ and all arrays are arranged in a linear shape with a half-wavelength separation between two adjacent array elements. During the ℓ-th pulse, $\ell = 1, \cdots, L$, the functions of radar and communication are operated simultaneously: 1) *Radar function*. The OFDM-type multicarrier signals with K subcarriers are transmitted to detect the position of the interest target (x_T, y_T). Note the frequency spacing Δf is assumed to be sufficiently large. 2) *Communication function*. The received signal during the $(\ell-1)$-th pulse, which contains the target information (x_T, y_T), is transmitted to the FC, where an estimation decision of the target information is made. Note that, motivated by the Amplify-and-Forward (AF) relay strategy [46], [47], the received signal is amplified firstly before transmission.

A. RECEIVED RADAR SIGNAL

Define $s_{k,j}, k = 1, \cdots, K$ as the transmitted waveform on the k-th subcarrier by the j-th IRCS, $j = 1, \cdots, J$; then, during the ℓ-th pulse, $\ell = 1, \cdots, L$, the received signal on the k-th subcarrier can be modeled as

$$\begin{aligned}\boldsymbol{y}_{r,k,j}(\ell) = &\bar{\alpha}\alpha'_{r,k,j}\boldsymbol{A}\left(\theta_{r,j}\right)\boldsymbol{u}_{k,j}s_{k,j}(\ell)\\ &+\sum_{\tilde{j}=1,\tilde{j}\neq j}^{J-1}\bar{\alpha}\alpha'_{I,k,\tilde{j}}\boldsymbol{A}\left(\varphi_{r,\tilde{j}},\theta_{r,j}\right)\boldsymbol{u}_{k,\tilde{j}}s_{m,k,\tilde{j}}(\ell)+\boldsymbol{n}_{r,k,j}(\ell),\end{aligned} \tag{1}$$

where $\theta_{r,j}$ and $\varphi_{r,\tilde{j}}$ denote the DOAs of the signals transmitted by the j-th and $\tilde{j}$-th IRCSs ($\tilde{j} \neq j$), respectively; $\boldsymbol{A}\left(\theta_{r,j}\right) = \boldsymbol{b}\left(\theta_{r,j}\right)\boldsymbol{a}^T\left(\theta_{r,j}\right)$ with $\boldsymbol{a}\left(\theta_{r,j}\right) \in \mathbb{C}^{N_T\times 1}$ and $\boldsymbol{b}\left(\theta_{r,j}\right) \in \mathbb{C}^{N_R\times 1}$ are the transmit/receive array steering vectors, respectively; $\boldsymbol{A}\left(\varphi_{r,\tilde{j}},\theta_{r,j}\right) = \boldsymbol{b}\left(\varphi_{r,\tilde{j}}\right)\boldsymbol{a}^T\left(\theta_{r,j}\right)$; $\boldsymbol{u}_{k,j}$ denotes the transmit beamformer on the k-th subcarrier associated with the j-th IRCS; $\bar{\alpha}$ denotes the target impulse response, which is assumed to be zero mean Gaussian random [48], [50], [51]; $\alpha'_{r,k,j}$ is the channel coefficient of the target associated with the k-th subcarrier; $\alpha'_{I,k,\tilde{j}}$ is the channel coefficient from the $\tilde{j}$-th IRCS to the target, to the j-th IRCS; $\boldsymbol{n}_{r,k,j} \in \mathbb{C}^{N_R\times 1}$ is additive white Gaussian noise (AWGN) vector with zero mean and covariance matrix $\sigma^2_{n,r,k,j}\boldsymbol{I}_{N_R}$.

The received signal $\boldsymbol{y}_{r,k,j}(t;\ell)$ is filtered through the receive beamformer $\boldsymbol{v}_{k,j} \in \mathbb{C}^{N_R\times 1}$, which outputs [18], [52], [53]:

$$\begin{aligned}y_{r,k,j}(\ell) = &\alpha_{r,k,j}\boldsymbol{v}^\dagger_{k,j}\boldsymbol{A}\left(\theta_{r,j}\right)\boldsymbol{u}_{k,j}s_{k,j}(\ell)\\ &+\sum_{\tilde{j}=1,\tilde{j}\neq j}^{J-1}\alpha_{I,k,\tilde{j}}\boldsymbol{v}^\dagger_{k,j}\boldsymbol{A}\left(\varphi_{r,\tilde{j}},\theta_{r,j}\right)\boldsymbol{u}_{k,\tilde{j}}s_{k,\tilde{j}}(\ell)\\ &+\boldsymbol{v}^\dagger_{k,j}\boldsymbol{n}_{r,k,j}(\ell),\end{aligned} \tag{2}$$

where $\alpha_{r,k,j}$ and $\alpha_{I,k,\tilde{j}}$ are the new parameters that integrate the target impulse response $\bar{\alpha}$, the channel coefficient $\alpha'_{r,k,j}$ and $\alpha'_{I,k,\tilde{j}}$, respectively [18].

After collecting the signals received from the K subcarriers into the vector $\boldsymbol{y}_{r,j} = \left[y_{r,1,j}, \cdots, y_{r,K,j}\right]^T$, we can write

$$\boldsymbol{y}_{r,j}(\ell) = \boldsymbol{\alpha}_{r,j}\boldsymbol{H}_j(\ell) + \sum_{\tilde{j}=1,\tilde{j}\neq j}^{J-1}\boldsymbol{\alpha}_{I,\tilde{j}}\boldsymbol{H}_{\tilde{j}j}(\ell) + \boldsymbol{V}_j, \tag{3}$$

where

$$\begin{aligned}\boldsymbol{H}_j(\ell) = &\,diag\left\{\boldsymbol{v}^\dagger_{1,j}\boldsymbol{A}\left(\theta_{r,j}\right)\boldsymbol{u}_{1,j}s_{1,j}(\ell),\cdots,\right.\\ &\left.\boldsymbol{v}^\dagger_{K,j}\boldsymbol{A}\left(\theta_{r,j}\right)\boldsymbol{u}_{K,j}s_{K,j}(\ell)\right\},\end{aligned} \tag{4a}$$

$$\begin{aligned}\boldsymbol{H}_{I,\tilde{j}}(\ell) = &\,diag\left\{\boldsymbol{v}^\dagger_{1,j}\boldsymbol{A}\left(\varphi_{r,\tilde{j}},\theta_{r,j}\right)\boldsymbol{u}_{1,\tilde{j}}s_{1,\tilde{j}}(\ell),\cdots,\right.\\ &\left.\boldsymbol{v}^\dagger_{K,j}\boldsymbol{A}\left(\varphi_{r,\tilde{j}},\theta_{r,j}\right)\boldsymbol{u}_{K,\tilde{j}}s_{K,\tilde{j}}(\ell)\right\},\end{aligned} \tag{4b}$$

$$\boldsymbol{\alpha}_{r,j} = vec\left\{\alpha_{r,1,j},\cdots,\alpha_{r,K,j}\right\}, \tag{4c}$$

$$\boldsymbol{\alpha}_{I,\tilde{j}} = vec\left\{\alpha_{I,1,\tilde{j}},\cdots,\alpha_{I,K,\tilde{j}}\right\}, \tag{4d}$$

$$\boldsymbol{V}_j = vec\left\{\boldsymbol{v}^\dagger_{1,j}\boldsymbol{n}_{r,1,j},\cdots,\boldsymbol{v}^\dagger_{K,j}\boldsymbol{n}_{r,K,j}\right\}. \tag{4e}$$

In the following, $\boldsymbol{\alpha}_{r,j}$ and $\boldsymbol{n}_{r,j}$ are modeled as circularly-symmetric Gaussian random vector with positive definite covariance matrices $\boldsymbol{\Sigma}_{r,j}$ and $\boldsymbol{\Sigma}_{I,\tilde{j}}$, respectively ($\boldsymbol{\alpha}_{r,j}$ and $\boldsymbol{\alpha}_{I,\tilde{j}}$ are mutually independent). Moreover, we assume a Swerling II fluctuation model for the radar cross-section of the prospective targets.

B. RECEIVED COMMUNICATION SIGNAL

To share the obtained information of interest target with the FC, we transmit the radar echoes signal $y_{r,k,j}$ to the FC. Before transmission, motivated by the AF relay strategy, we amplify $y_{r,k,j}$ and the amplification factor $G_{k,j}$ is selected so that the following is satisfied:

$$E\left\{\left|G_{k,j}y_{r,k,j}(\ell-1)\right|^2\right\} = E\left\{\left|s_{k,j}(\ell)\right|^2\right\} = \mathcal{P}_{\max}, \tag{5}$$

where $\mathcal{P}_{\max}$ denotes the available transmit power. Combining Eq. (2), we have

$$\begin{aligned}G_{k,j} = &\left|s_{k,j}(\ell)\right|\left(\sigma^2_{\alpha,r,k,j}\eta_{k,j}(\ell)\right.\\ &\left.+\sigma^2_{I,k,\tilde{j}}\tilde{\eta}_{k,j}(\ell-1)+\sigma^2_{n,r,k,j}\boldsymbol{v}^\dagger_{k,j}\boldsymbol{v}_{k,j}\right)^{-1/2},\end{aligned} \tag{6}$$

where

$$\eta_{k,j}(\ell-1)=\left|\boldsymbol{v}_{k,j}^{\dagger}\boldsymbol{A}\left(\theta_{r,j}\right)\boldsymbol{u}_{k,j}s_{k,j}(\ell-1)\right|^2, \tag{7}$$

$$\tilde{\eta}_{k,j}(\ell-1)=\sum_{\tilde{j}=1,\tilde{j}\neq j}^{J-1}\left|\boldsymbol{v}_{k,j}^{\dagger}\boldsymbol{A}\left(\varphi_{r,\tilde{j}},\theta_{r,j}\right)\boldsymbol{u}_{k,j}s_{k,\tilde{j}}(\ell-1)\right|^2. \tag{8}$$

During the ℓ-th PRI, the quantized samples at the j-th IRCS is transmitted to the FC located at the direction $\theta_{c,j}$. Then, the received signal at the FC from the j-th IRCS, $\boldsymbol{y}_{c,k}(t;\ell)\in\mathbb{C}^{N_R\times 1}$, can be written as

$$\begin{aligned}&\boldsymbol{y}_{c,k,j}(t;\ell)\\&\quad=\alpha_{c,k,j}\boldsymbol{A}\left(\theta_{c,j}\right)\boldsymbol{u}_{k,j}G_{k,j}y_{r,k,j}(\ell-1)+\boldsymbol{n}_{c,k}(\ell)\end{aligned} \tag{9}$$

for $k=1,\cdots,K$, and $j=1,\cdots,J$, where $\alpha_{c,k,j}$ denotes the channel coefficient on the k-th subcarrier of the link between the j-th IRCS and the FC; $\boldsymbol{w}_k\in\mathbb{C}^{N_R\times 1}$ is the communication receive beamformer on the k-th subcarrier; finally, $\boldsymbol{n}_{c,k}$ is the AWGN on the k-th subcarrier with zero mean and covariance matrix $\sigma_{n,c,k}^2\boldsymbol{I}_{N_R}$.

The received signal $\boldsymbol{y}_{c,k}(t;\ell)$ filtered through the receive beamformer $\boldsymbol{w}_k\in\mathbb{C}^{N_R\times 1}$ outputs [18], [52], [53]:

$$\begin{aligned}&y_{c,k,j}(t;\ell)\\&\quad=\alpha_{c,k,j}\boldsymbol{w}_{k,j}^{\dagger}\boldsymbol{A}\left(\theta_{c,j}\right)\boldsymbol{u}_{k,j}G_{k,j}y_{r,k,j}(\ell-1)+\boldsymbol{w}_{k,j}^{\dagger}\boldsymbol{n}_{c,k}(\ell).\end{aligned} \tag{10}$$

After collecting the signals received from the K subcarriers into the vector $\boldsymbol{y}_{c,j}=\left[y_{c,1,j},\cdots,y_{c,K,j}\right]^T$, we can write

$$\boldsymbol{y}_{c,j}(\ell)=\boldsymbol{\alpha}_{c,k,j}\boldsymbol{\Phi}_j(\ell-1)+\boldsymbol{W}_j, \tag{11}$$

where

$$\begin{aligned}\boldsymbol{\Phi}_j(\ell-1)&=diag\{\boldsymbol{w}_1^{\dagger}\boldsymbol{A}\left(\theta_{c,j}\right)\boldsymbol{u}_{1,j}y_{r,1,j}(\ell-1),\\&\qquad\cdots,\boldsymbol{w}_K^{\dagger}\boldsymbol{A}\left(\theta_{c,j}\right)\boldsymbol{u}_{K,j}y_{r,K,j}(\ell-1)\},\end{aligned} \tag{12a}$$

$$\boldsymbol{\alpha}_{c,j}=vec\{\alpha_{c,1,j},\cdots,\alpha_{c,K,j}\}, \tag{12b}$$

$$\boldsymbol{G}_j=diag\{G_{1,j},\cdots,G_{K,j}\}, \tag{12c}$$

$$\boldsymbol{W}_j=vec\{\boldsymbol{w}_{1,j}^{\dagger}\boldsymbol{n}_{c,1},\cdots,\boldsymbol{w}_{K,j}^{\dagger}\boldsymbol{n}_{c,K}\}. \tag{12d}$$

In the following, we model $\boldsymbol{\alpha}_{c,j}$ as circularly-symmetric Gaussian random vectors with covariance matrix $\boldsymbol{\Sigma}_{c,j}$. Also, the random vectors $\boldsymbol{\alpha}_{c,j}$ and $\boldsymbol{n}_{c,k}$ are mutually independent.

Without loss of generality, we assume that the received signals from all the J IRCSs are mutually independent. Then, combining $\{\boldsymbol{y}_{c,1}(\ell),\cdots,\boldsymbol{y}_{c,K}(\ell)\}$, a global estimation can be constructed:

$$z_c^{glo}(\ell)=f\left(\boldsymbol{y}_{c,1}(\ell),\cdots,\boldsymbol{y}_{c,K}(\ell)\right), \tag{13}$$

where $f(\cdot)$ is an approach to fuse the received signals, which depends on the selection of fusion rule, and we will discuss it later in detail.

Remark: The amount of radar echoes data is related to the sampling interval, and scanning speed [54]. Meanwhile, the maximum data of the adopted technique is related to the number of subcarrier K, adopted waveform M and allowable sidelobe levels Q. During each pulse, the maximum data is $KM\log_2 Q$ *bit* [26]. Data retention will happen if data rate cannot meet the requirement of data transmission, for instance, the samples at the J IRCSs cannot be transmitted to the FC timely. As a consequence, the performance will degrade. The CRB of localization estimation for the IRCS network taking into account the data retention will be investigated in the future.

III. CRBs OF TOA AND DOA ESTIMATION

In this section, we first derive the CRBs of TOA and DOA estimation for the IRCS. Then, we iteratively update the $u_{k,j}$ and $\boldsymbol{v}_{k,j}$ to maximize the SINR of radar. Also, the closed-form of the optimal communication receive beamformer $\boldsymbol{w}_{c,k,j}$ is derived.

A. CRBs OF TOA AND DOA ESTIMATION FOR IRCS

For the observed communication signal presented in (11), in view of the AWGN, the probability density function (pdf) of $\boldsymbol{y}_{c,j}(\ell)$ conditioned on τ and θ is

$$p\left(\boldsymbol{y}_{c,j};\tau,\theta\right)=\frac{\exp\left(-\boldsymbol{y}_{c,j}{}^{\dagger}\left(\boldsymbol{\Phi}_j\boldsymbol{\Sigma}_{c,j}\boldsymbol{\Phi}_j^{\dagger}+\boldsymbol{D}_j\right)^{-1}\boldsymbol{y}_{c,j}\right)}{\pi^K det\left(\boldsymbol{\Phi}_j\boldsymbol{\Sigma}_{c,j}\boldsymbol{\Phi}_j^{\dagger}+\boldsymbol{D}_j\right)}, \tag{14}$$

where $\boldsymbol{D}_j=\boldsymbol{W}_j\boldsymbol{W}_j^{\dagger}$.

Defining $\hat{\tau}_j$ and $\hat{\theta}_j$ as the TOA and DOA data measured by the j-th IRCS, the TOA/DOA maximum likelihood (ML) estimation can be found by jointly searching over (τ_j,θ_j) to maximize $p\left(\boldsymbol{y}_{c,j};\tau,\theta\right)$. The joint ML estimator is unbiased and the CRB for (τ_j,θ_j) is a function of the signal-to-noise ratio (SNR) at the receiver [42]–[45]. Therefore, CRBs of TOA and DOA estimation, i.e., $\mathcal{C}_{\tau,j,R+C}$ and $\mathcal{C}_{\theta,j,R+C}$, can be given by

$$\mathcal{C}_{\tau,j,R+C}=\frac{6tr\left(\boldsymbol{D}_j^{-1/2}\boldsymbol{\Phi}_j\boldsymbol{\Sigma}_{c,j}\boldsymbol{\Phi}_j^{\dagger}\boldsymbol{D}_j^{-1/2}\right)^{-1}}{N_R\left(K\Delta f\right)^2}, \tag{15}$$

$$\mathcal{C}_{\theta,j,R+C}=\frac{3tr\left(\boldsymbol{D}_j^{-1/2}\boldsymbol{\Phi}_j\boldsymbol{\Sigma}_{c,j}\boldsymbol{\Phi}_j^{\dagger}\boldsymbol{D}_j^{-1/2}\right)^{-1}}{\pi^2\sin^2\theta_{r,j}N_R\left(N_R-1\right)\left(N_R+1\right)}. \tag{16}$$

In the case of sufficiently large frequency spacing Δf, we have

$$\boldsymbol{\Sigma}_{r,j}=diag\left\{\sigma_{\alpha,r,1,j}^2,\ldots,\sigma_{\alpha,r,K,j}^2\right\}, \tag{17}$$

$$\boldsymbol{\Sigma}_{I,\tilde{j}}=diag\{\sigma_{I,1,\tilde{j}}^2,\ldots,\sigma_{I,K,\tilde{j}}^2\}, \tag{18}$$

$$\boldsymbol{\Sigma}_{c,j}=diag\left\{\sigma_{\alpha,c,1,j}^2,\ldots,\sigma_{\alpha,c,K,j}^2\right\}. \tag{19}$$

Then, the communication SNR on the k-th subcarrier, i.e., $\Gamma_{c,k,j}$, can be given by

$$\Gamma_{c,k,j}=\frac{\sigma_{\alpha,c,k,j}^2\left|\boldsymbol{w}_{k,j}^{\dagger}\boldsymbol{A}\left(\theta_{c,j}\right)\boldsymbol{u}_{k,j}s_{k,j}\right|^2}{\sigma_{n,c,k}^2\boldsymbol{w}_{k,j}^{\dagger}\boldsymbol{w}_{k,j}}, \tag{20}$$

meanwhile, the radar SINR on the k-th subcarrier, i.e., $\Gamma_{r,k,j}$, is written as

$$\Gamma_{r,k,j} = \frac{\sigma_{\alpha,r,k,j}^2 \left|\boldsymbol{v}_{k,j}^{\dagger}\boldsymbol{A}\left(\theta_{r,j}\right)\boldsymbol{u}_{k,j}s_{k,j}\right|^2}{\sigma_{I,k,\tilde{j}}^2 F_j + \sigma_{n,r,k,j}^2 \boldsymbol{v}_{k,j}^{\dagger}\boldsymbol{v}_{k,j}}, \tag{21}$$

where

$$F_j = \sum\nolimits_{\tilde{j}=1,\tilde{j}\neq j}^{J-1} \left|\boldsymbol{v}_{k,j}^{\dagger}\boldsymbol{A}\left(\varphi_{r,\tilde{j}},\theta_{r,j}\right)\boldsymbol{u}_{k,j}s_{m,k,\tilde{j}}\right|^2. \tag{22}$$

Therefore, $\mathcal{C}_{\tau,j,R+C}$ and $\mathcal{C}_{\theta,j,R+C}$ can be further given in the following Proposition.

Proposition 1: In the case of large frequency spacing, the CRBs of TOA and DOA estimation, i.e., $\mathcal{C}_{\tau,j,R+C}$ and $\mathcal{C}_{\theta,j,R+C}$, can be, respectively, given by

$$\mathcal{C}_{\tau,j,R+C} = \sum_{k=1}^{K} \frac{6\left(\Gamma_{c,k,j}^{-1} + \Gamma_{r,k,j}^{-1}\left(1+\Gamma_{c,k,j}^{-1}\right)\right)}{N_R\left(K\Delta f\right)^2}, \tag{23}$$

$$\mathcal{C}_{\theta,j,R+C} = \sum_{k=1}^{K} \frac{3\left(\Gamma_{c,k,j}^{-1} + \Gamma_{r,k,j}^{-1}\left(1+\Gamma_{c,k,j}^{-1}\right)\right)}{\pi^2\sin^2\theta_{r,j}N_R\left(N_R-1\right)\left(N_R+1\right)}. \tag{24}$$

Proof: See Appendix A.

Next, we introduce the method how to optimize the radar transmit/receive beamformer $\boldsymbol{u}_{k,j}/\boldsymbol{v}_{k,j}$ and the communication receive beamformer $\boldsymbol{w}_{k,j}$.

B. TRANSMIT/RECEIVE BEAMFORMER OPTIMIZATION

1) ITERATIVE $u_{k,j}$ AND $v_{k,j}$ OPTIMIZATION

The ITRB technique iteratively optimizes $\boldsymbol{u}_k$ and $\boldsymbol{v}_k$ in $\Gamma_{r,k,j}$ choosing the following two criteria: 1) Maximize $\Gamma_{r,k,j}$ with the constraint of the available transmit power $\mathcal{P}_{\max}$; 2) enable information streams toward the FC without affecting the performance of radar detection. This is equivalent to the following optimization problem:

$$\begin{aligned}
&\max_{\boldsymbol{u}_{k,j},\boldsymbol{v}_{k,j}} \frac{\left|\boldsymbol{v}_{k,j}^{\dagger}\boldsymbol{A}\left(\theta_{r,j}\right)\boldsymbol{u}_{k,j}\right|^2}{\sigma_{I,k,\tilde{j}}^2 F_j + \sigma_{n,r,k,j}^2 \boldsymbol{v}_{k,j}^{\dagger}\boldsymbol{v}_{k,j}} \\
&s.t.\ C1: \sum\nolimits_{k=1}^{K} \|\boldsymbol{u}_k\|^2 \le \mathcal{P}_{\max}, \\
&\quad C2: \left|\boldsymbol{a}^T\left(\theta\right)\boldsymbol{u}_{k,j}\right| \le \Delta_{SLL}, \quad \theta \in \bar{\Theta} \\
&\quad C3: \boldsymbol{a}^T\left(\phi_{c,j}\right)\boldsymbol{u}_{k,j} = \Delta_q, \quad 1 \le q \le Q
\end{aligned} \tag{25}$$

where Δ_{SLL} is the maximum power that can be radiated towards the sidelobe directions included in the set $\bar{\Theta}$; Δ_q denotes the sidelobe level towards the FC direction $\phi_{c,j}$ and we assume $\Delta_q \le \Delta_{SLL}$. Such sidelobe levels are chosen from a pre-assigned codebook containing Q codewords, say $\mathcal{D} = \{\Delta_1, \cdots, \Delta_Q\}$. Each SLL of all the Q SLLs is mapped to a unique communication symbol, thereby enabling the FC receiver to receive the information message by determining which SLL was transmitted.

The joint $\boldsymbol{u}_{k,j}$ and $\boldsymbol{v}_{k,j}$ optimization problem in (25) is solved by a sequential optimization algorithm. That is, we first optimize $\boldsymbol{v}_{k,j}$ for a fixed $\boldsymbol{u}_{k,j}$ and then optimize $\boldsymbol{u}_{k,j}$ for a fixed $\boldsymbol{v}_{k,j}$. Specifically, choosing the maximization of $\Gamma_{r,k,j}$ as optimization criterion, we obtain the optimal $\boldsymbol{v}_{k,j}$ (with fixed $\boldsymbol{u}_{k,j}$) by solving

$$\max_{\boldsymbol{v}_{k,j}} \frac{\left|\boldsymbol{v}_{k,j}^{\dagger}\boldsymbol{A}\left(\theta_{r,j}\right)\boldsymbol{u}_{k,j}\right|^2}{\boldsymbol{v}_{k,j}^{\dagger}\boldsymbol{F}_{\boldsymbol{u},j}\boldsymbol{v}_{k,j} + \sigma_{n,r,k,j}^2\boldsymbol{v}_{k,j}^{\dagger}\boldsymbol{v}_{k,j}}, \tag{26}$$

where

$$\boldsymbol{F}_{\boldsymbol{u},j} = \sum\nolimits_{\tilde{j}=1,\tilde{j}\neq j}^{J-1} \sigma_{I,k,\tilde{j}}^2 |s_{k,\tilde{j}}|^2 \boldsymbol{A}^{\dagger}\left(\varphi_{r,\tilde{j}},\theta_{r,j}\right)\boldsymbol{u}_{k,j}\boldsymbol{u}_{k,j}^{\dagger}\boldsymbol{A}\left(\varphi_{r,\tilde{j}},\theta_{r,j}\right). \tag{27}$$

The $\boldsymbol{v}_{k,j}$ optimization problem in (26) can be recast as the minimum variance distortionless response (MVDR) problem [49], namely

$$\begin{aligned}
&\min_{\boldsymbol{v}_{k,j}} \boldsymbol{v}_{k,j}^{\dagger}\left(\boldsymbol{F}_{\boldsymbol{u},j} + \sigma_{n,r,k,j}^2\boldsymbol{I}_{N_R}\right)\boldsymbol{v}_{k,j} \\
&s.t.\ C1: \boldsymbol{v}_{k,j}^{\dagger}\boldsymbol{A}\left(\theta_{r,j}\right)\boldsymbol{u}_{k,j} = 1.
\end{aligned} \tag{28}$$

It follows from problem (28) that

$$\boldsymbol{v}_{k,j} = \frac{\left(\boldsymbol{F}_{\boldsymbol{u},j} + \sigma_{n,r,k,j}^2\boldsymbol{I}_{N_R}\right)^{-1}\boldsymbol{A}\left(\theta_{r,j}\right)\boldsymbol{u}_{k,j}}{\left(\boldsymbol{A}\left(\theta_{r,j}\right)\boldsymbol{u}_{k,j}\right)^{\dagger}\left(\boldsymbol{F}_{\boldsymbol{u},j} + \sigma_{n,r,k,j}^2\boldsymbol{I}_{N_R}\right)^{-1}\boldsymbol{A}\left(\theta_{r,j}\right)\boldsymbol{u}_{k,j}}. \tag{29}$$

Next, with fixed $\boldsymbol{v}_{k,j}$, the optimal transmit beamformer $\boldsymbol{u}_{u,j}$ is obtained by solving the following optimization problem:

$$\begin{aligned}
&\max_{\boldsymbol{u}_{k,j}} \frac{\left|\boldsymbol{v}_{k,j}^{\dagger}\boldsymbol{A}\left(\theta_{r,j}\right)\boldsymbol{u}_{k,j}\right|^2}{\boldsymbol{u}_{k,j}^{\dagger}\boldsymbol{F}_{\boldsymbol{v},j}\boldsymbol{u}_{k,j} + \sigma_{n,r,k,j}^2\boldsymbol{v}_{k,j}^{\dagger}\boldsymbol{v}_{k,j}} \\
&s.t.\ C1: \sum\nolimits_{k=1}^{K} \|\boldsymbol{u}_k\|^2 \le \mathcal{P}_{\max}, \\
&\quad C2: \left|\boldsymbol{a}^T\left(\theta\right)\boldsymbol{u}_{k,j}\right| \le \Delta_{SLL}, \quad \theta \in \bar{\Theta} \\
&\quad C3: \boldsymbol{a}^T\left(\phi_{c,j}\right)\boldsymbol{u}_{k,j} = \Delta_q, \quad 1 \le q \le Q
\end{aligned} \tag{30}$$

where

$$\boldsymbol{F}_{\boldsymbol{v},j} = \sum\nolimits_{\tilde{j}=1,\tilde{j}\neq j}^{J-1} \sigma_{I,k,\tilde{j}}^2 |s_{k,\tilde{j}}|^2 \boldsymbol{A}^{\dagger}\left(\varphi_{r,\tilde{j}},\theta_{r,j}\right)\boldsymbol{v}_{k,j}\boldsymbol{v}_{k,j}^{\dagger}\boldsymbol{A}\left(\varphi_{r,\tilde{j}},\theta_{r,j}\right). \tag{31}$$

Then, problem (30) can be recast as

$$\begin{aligned}
&\min_{\boldsymbol{u}_{k,j}} \boldsymbol{u}_{k,j}^{\dagger}\boldsymbol{F}_{\boldsymbol{v},j}\boldsymbol{u}_{k,j} + \sigma_{n,r,k,j}^2\boldsymbol{v}_{k,j}^{\dagger}\boldsymbol{v}_{k,j} \\
&s.t.\ C1: \sum\nolimits_{k=1}^{K} \|\boldsymbol{u}_k\|^2 \le \mathcal{P}_{\max}, \\
&\quad C2: \boldsymbol{v}_{k,j}^{\dagger}\boldsymbol{A}\left(\theta_{r,j}\right)\boldsymbol{u}_{k,j} = \|u_k\|^2, \\
&\quad C3: \left|\boldsymbol{a}^T\left(\theta\right)\boldsymbol{u}_{k,j}\right| \le \Delta_{SLL}, \quad \theta \in \bar{\Theta} \\
&\quad C4: \boldsymbol{a}^T\left(\phi_{c,j}\right)\boldsymbol{u}_{k,j} = \Delta_q, \quad 1 \le q \le Q
\end{aligned} \tag{32}$$

The above optimization problem is convex and the convex optimization toolbox CVX [55] in MATLAB will be used. The $\boldsymbol{u}_{k,j}$ and $\boldsymbol{v}_{k,j}$ iteration process is stopped when the $\Gamma_{r,k,j}$ improvement is no more than a pre-assigned number δ. It is obvious that the objective function is bounded and nondecreasing in each iteration, which ensures the convergence due to the monotone convergence theorem [56].

2) COMMUNICATION RECEIVE BEAMFORMER $w_{c,k,j}$ OPTIMIZATION

Choosing the maximization of $\Gamma_{c,k,j}$ as optimization criterion, the $\boldsymbol{w}_{k,j}$ can be optimized by solving the following optimization problem:

$$\max_{\boldsymbol{w}_{k,j}} \frac{\left|\boldsymbol{w}_{k,j}^{\dagger}\boldsymbol{A}\left(\theta_{c,j}\right)\boldsymbol{u}_{k,j}\right|^2}{\boldsymbol{w}_{k,j}^{\dagger}\boldsymbol{w}_{k,j}} \tag{33}$$

The above optimization problem can be recast as

$$\begin{aligned} &\min_{\boldsymbol{w}_{k,j}} \boldsymbol{w}_{k,j}^{\dagger}\boldsymbol{w}_{k,j} \\ &s.t.\ C1 : \boldsymbol{w}_{k,j}^{\dagger}\boldsymbol{A}\left(\theta_{c,j}\right)\boldsymbol{u}_{k,j} = 1. \end{aligned} \tag{34}$$

Similarly, the optimal $\boldsymbol{w}_{c,k,j}$ for (34) is given by

$$\boldsymbol{w}_{k,j} = \frac{\boldsymbol{A}\left(\theta_{c,j}\right)\boldsymbol{u}_{k,j}}{\left(\boldsymbol{A}\left(\theta_{c,j}\right)\boldsymbol{u}_{k,j}\right)^{\dagger}\boldsymbol{A}\left(\theta_{c,j}\right)\boldsymbol{u}_{k,j}}. \tag{35}$$

IV. CRB OF LOCALIZATION ESTIMATION

In this section, the CRB of localization estimation is derived by using the hybrid TOA/DOA measurement. Then, the CRB of localization estimation fused from J IRCSs is derived at the FC by adopting the linear fusion rule.

A. CRB OF LOCALIZATION ESTIMATION FOR INDIVIDUAL IRCS

For the j-th IRCS, let $\tau_{r,j}$ and $\theta_{r,j}$ denote the actual TOA and DOA, respectively; then, the estimated TOA and DOA can be, respectively, given by [43], [44], [57]

$$\hat{\tau}_{r,j} = \tau_{r,j} + \Delta\tau_{r,j}, \tag{36}$$

$$\hat{\theta}_{r,j} = \theta_{r,j} + \Delta\theta_{r,j}, \tag{37}$$

where $\Delta\tau_{r,j}$ and $\Delta\theta_{r,j}$ denote the estimation errors of $\tau_{r,j}$ and $\theta_{r,j}$, respectively. Thus, after defining $\boldsymbol{p}_j = (x_j, y_j)$ and $\boldsymbol{p}_T = (x_T, y_T)$ as the positions of the j-th IRCS and target, respectively, the localization estimation $\hat{\boldsymbol{p}}_T = (\hat{x}_T, \hat{y}_T)$ can be given as follows

$$\begin{aligned} \hat{x}_T &= x + c\hat{\tau}_{r,j}\cos\hat{\theta}_{r,j} \\ &= x + c\left(\tau_{r,j} + \Delta\tau_{r,j}\right)\cos\left(\theta_{r,j} + \Delta\theta_{r,j}\right), \end{aligned} \tag{38}$$

$$\begin{aligned} \hat{y}_T &= y + c\hat{\tau}_{r,j}\sin\hat{\theta}_{r,j} \\ &= y + c\left(\tau_{r,j} + \Delta\tau_{r,j}\right)\sin\left(\theta_{r,j} + \Delta\theta_{r,j}\right), \end{aligned} \tag{39}$$

where c denotes the speed of light. Using the following approximations: $\Delta\theta_{r,j}$ and $\Delta\tau_{r,j}$ are small enough such that $\cos\Delta_{r,j}\theta_{r,j} \simeq 1$, $\sin\Delta\theta_{r,j} \simeq \theta_{r,j}$ and $\Delta\theta_{r,j}\Delta\tau_{r,j} \approx 0$, we have

$$\hat{x}_T - x_j \simeq -d_{r,j}\Delta\theta_{r,j}\sin\theta_{r,j} + c\Delta\tau_{r,j}\cos\theta_{r,j}, \tag{40}$$

$$\hat{y}_T - y_j \simeq d_{r,j}\Delta\theta_{r,j}\cos\theta_{r,j} + c\Delta\tau_{r,j}\sin\theta_{r,j}, \tag{41}$$

where $d_{r,j} = c\tau_{r,j}$ denotes the detection range. Then, the mean square error (MSE) of x_T estimation ψ_{x_T} can be given as follows

$$\begin{aligned} \psi_{x_T} &= E\left\{\left\|\hat{x}_T - x_T\right\|^2\right\} \\ &\simeq d_{r,j}^2\sin^2\theta_{r,j}E\left\{\left\|\hat{\theta}_{r,j} - \theta_{r,j}\right\|^2\right\} \\ &\quad + c^2\cos^2\theta_{r,j}E\left\{\left\|\hat{\tau}_{r,j} - \tau_{r,j}\right\|^2\right\} \\ &\geq d_{r,j}^2\sin^2\theta_r\mathcal{C}_{\theta,j,R+C} + c^2\cos^2\theta_{r,j}\mathcal{C}_{\tau,j,R+C}, \end{aligned} \tag{42}$$

where $\mathcal{C}_{\tau,j,R+C}$ and $\mathcal{C}_{\theta,j,R+C}$ are given by Eqs. (23) and (24), respectively. Similarly, the MSE of y_T estimation ψ_{y_T} can be determined as follows

$$\begin{aligned} \psi_{y_T} &= E\left\{\left\|\hat{y}_T - y_T\right\|^2\right\} \\ &\geq d_{r,j}^2\cos^2\theta_{r,j}\mathcal{C}_{\theta,j,R+C} + c^2\sin^2\theta_{r,j}\mathcal{C}_{\tau,j,R+C}. \end{aligned} \tag{43}$$

Thus, after deriving the MSEs of x_T and y_T estimations, i.e., ψ_{x_T} and ψ_{y_T}, the MSE of localization estimation $\psi_{\boldsymbol{p}_T}$ can be given by

$$\begin{aligned} \psi_{\boldsymbol{p}_T} &= E\left\{\left\|\widehat{\boldsymbol{p}}_T - \boldsymbol{p}_T\right\|^2\right\} \\ &= E\left\{\left(\hat{x}_T - x_T\right)^2 + \left(\hat{y}_T - y_T\right)^2\right\} \\ &= J_{x_T} + J_{y_T} \\ &\geq d_{r,j}^2\mathcal{C}_{\theta,j,R+C} + c^2\mathcal{C}_{\tau,j,R+C}. \end{aligned} \tag{44}$$

As a result, the CRB of localization estimation, which is the minimum MSE (MMSE), can be given by

$$\begin{aligned} \mathcal{C}_{\boldsymbol{p}_T,j,R+C} &= \min J_{\boldsymbol{u}_T} \\ &= d_{r,j}^2\mathcal{C}_{\theta,j,R+C} + c^2\mathcal{C}_{\tau,j,R+C}. \end{aligned} \tag{45}$$

It can be seen that $\mathcal{C}_{\boldsymbol{p}_T,j,R+C}$ is related to the distance between the IRCS and target and large $d_{r,j}$ considerably magnifies the errors in position estimation. Meanwhile, form Eq. (16) we can see that the $\theta_{r,j}$ has considerably impact on $\mathcal{C}_{\boldsymbol{p}_T,j,R+C}$. Then, it's clearly that the positioning accuracy is related to $\theta_{r,j}$. The estimation is most accurate when $\theta_{r,j} = 90°$ because $\sin(90°) = 1$ and least accurate in case $\theta_{r,j}$ equals $0°$ or $180°$ because $\sin(0°) = 0$ or $\sin(180°) = 0$. Thus, even when the IRCS is very close to the target, the positioning estimation error would still be large.

B. FUSED CRB OF LOCALIZATION ESTIMATION

In this subsection, we consider the fusion technique for localization estimation problem. Adopting linear fusion rule [58], a global decision $\mathcal{C}_{\boldsymbol{p}_T,R+C}^{glo}$ is made combining all the J estimation results $\left\{\mathcal{C}_{\boldsymbol{p}_T,1,R+C}, \cdots, \mathcal{C}_{\boldsymbol{p}_T,J,R+C}\right\}$ (which are mutually independent). The linear fusion rule is to get the $\mathcal{C}_{\boldsymbol{p}_T,R+C}^{glo}$ by linearly combining all the J estimation results:

$$\mathcal{C}_{\boldsymbol{p}_T,R+C}^{glo}(\boldsymbol{\omega}) = \sum_{j=1}^{J}\omega_j\mathcal{C}_{\boldsymbol{p}_T,j,R+C}, \tag{46}$$

where $\boldsymbol{\omega} := \{\omega_1, \omega_2, \cdots, \omega_J\}$ are linear weights satisfying $\sum_{j=1}^{J}\omega_j = 1$, $\mathcal{C}_{\boldsymbol{p}_T,j,R+C}$ is the CRB of localization estimation according to the received signal from jth IRCS, which has been derived in (45). For optimal linear fusion, the linear weights $\boldsymbol{\omega}$ are critical parameters for minimizing the fused CRB. Subject (46) to a normalization

constraint $\sum_{j=1}^{J}\omega_j = 1$, $\mathcal{C}_{\boldsymbol{p}_T,j,R+C}$ to avoid trivial solutions, the fused CRB of localization estimation can be given by

$$\begin{aligned}\mathcal{C}^{glo}_{\boldsymbol{p}_T,R+C} &= \min_{\boldsymbol{\omega}} \mathcal{C}_{\boldsymbol{p}_T,j,R+C}(\boldsymbol{\omega}) \\ &= \left(\sum_{j=1}^{J}\left(\mathcal{C}_{\boldsymbol{p}_T,j,R+C}\right)^{-1}\right)^{-1} \\ &= \left(\sum_{j=1}^{J}\left(d^2_{r,j}\mathcal{C}_{\theta,j,R+C} + c^2\mathcal{C}_{\tau,j,R+C}\right)^{-1}\right)^{-1}, \quad (47)\end{aligned}$$

which corresponds to setting the optimal weights as [58]

$$\omega_j = \frac{\left(\mathcal{C}_{\boldsymbol{p}_T,j,R+C}\right)^{-1}}{\sum_{j=1}^{J}\left(\mathcal{C}_{\boldsymbol{p}_T,j,R+C}\right)^{-1}}, \quad j = 1, 2, \cdots, J. \quad (48)$$

V. NUMERICAL EXAMPLES

In this section, we provide simulation results to quantify the estimation performances of the IRCS. Note that the estimation performance of the TRS is also studied as a contrast.[2] We assume a network consisting of $J = 3$ IRCSs and each IRCS equips with a uniform linear transmit array consisting of $N = 15$ antennas. Here, the number of subcarrier and subcarrier spacing are set to be $K = 64$ and $\Delta f = 0.25$ M, respectively. The variances of radar and communication are normalized as $\sigma^2_{n,r} = \sigma^2_{n,c} = 1$. The strength of the desired and interference signals, indicated by $\sigma^2_{\alpha,r}$ and σ^2_I, are set as $\sigma^2_{\alpha,r} = \sigma^2_I = 0.1$. The average performances are obtained by 100 trials of channel realization.

Transmit and receive beamformers of radar are designed to focus their individual mainbeams towards the direction $\theta_r = 90°$ in the presence of 2 interference signals locating in directions $\varphi_{r,1} = 140°$ and $\varphi_{r,2} = 160°$. For all other sidelobe directions, the SLLs are controlled by choosing $\delta_u = -15$ dB, all relative to the mainbeam. We assume communication message of $\log_2(Q) = \log_2(4) = 2$ bits are delivered towards the FC direction located in the sidelobe region during each PRI. For the sidelobe directions, the SLLs are constrained by $\Delta_{SLL} = -15$ dB, relative to the mainbeam. Also, the communication receive beamformer is designed to focus mainbeam towards the direction $\theta_c = 90°$. In the simulation, 100 trials of channel realization are utilized to obtain average results.

Fig. 2 depicts the transmit power distribution versus spatial angle for all the $Q = 4$ transmit beampatterns which focus their mainbeams towards the radar operation direction $\theta_r = 90°$ and sidelobe towards the communication direction $\phi_c = 120°$ and interference resource directions $\varphi_{r,1} = 140°$ and $\varphi_{r,2} = 160°$. We can see that, as expected, the pattern within the mainbeam of the transmit beampatterns are almost the same, which implies that the performance of radar detection would not be affected. The SLLs of the transmit beampattern in the direction $\phi_c = 120°$ are constrained to be at $\Delta_1 = -20$ dB, $\Delta_2 = -25$ dB, $\Delta_3 = -30$ dB and $\Delta_4 = -35$ dB, all relative to the mainbeam. These $Q = 4$ different SLLs towards the direction of FC are separated from each other and enabling the FC to detect which transmit SLL was adopted and, in turn, determine the corresponding information message. As a result, communication symbols can be embedded in the transmit radar waveform without affecting the performance of the radar.

[2]The CRB of localization estimation for individual TRS and the fused result from different TRSs are presented in Appendix B.

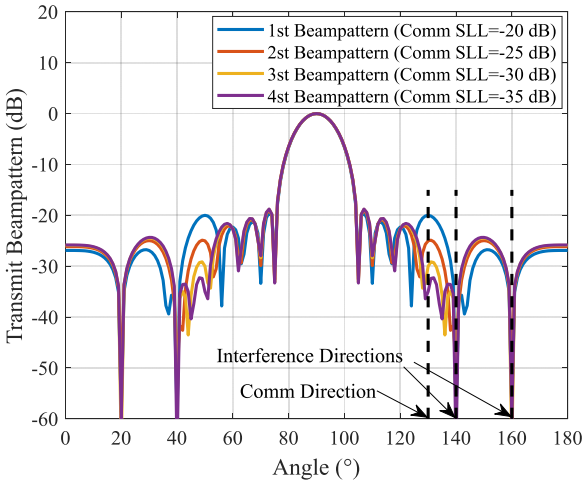

FIGURE 2. Normalized transmit power distribution versus spatial angle for all the $Q = 4$ transmit vectors.

Fig. 3 depicts the power allocation results under $\mathcal{P}_{\max} = 10$ kW. As shown in Fig. 3(a), part of subcarriers, such as subcarriers 4, 5, 7, are bad for radar, then, these subcarriers are not used, i.e., the allocated power is zero, as shown in Fig. 3(b). That is, according to the conditions of radar subcarriers, the available transmit power is adaptively allocated to the $K = 64$ subcarriers to maximize the radar SINR.

Fig. 4 depicts the root-mean-square error (RMSE) of DOA estimation versus transmit power $\mathcal{P}_{\max}$ under $\sigma^2_{\alpha,c} = 1$. We can see that, as discussed in Section IV-A, spatial angle θ_r has a considerably impact on the performance of DOA estimation. The estimation is the most accuracy when angle $\theta_r = 90°$. For all the three cases $\theta_r = 90°$, $40°$, and $115°$, the ITRB technique achieves a better estimation accuracy, i.e., smaller RMSE, compared with the TB technique adopted in [22]. This is because the ITRB technique iteratively updates the transmit and receive beamformers. We can also see that, as expected, the larger transmit power $\mathcal{P}_{\max}$ is, the better accuracy of DOA estimation is.

Fig. 5 depicts the RMSE of TOA estimation versus transmit power $\mathcal{P}_{\max}$. We can see that, as expected, the larger transmit power $\mathcal{P}_{\max}$ is, the better accuracy of TOA estimation is. Comparing the cases of the IRCS and TRS, the RMSE for the IRCS is worse than that for the TRS, since the additional errors, i.e., the communication transmission error. We can also see that, with larger variance $\sigma^2_{\alpha,c}$ (which implies better communication channel condition), the accuracy of TOA estimation is better. Similar to the DOA estimation, the ITRB

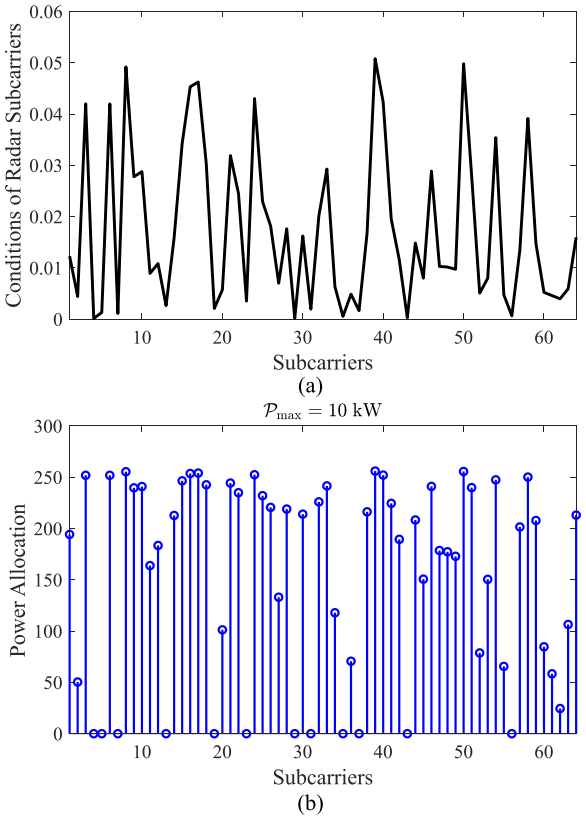

FIGURE 3. Power allocation results. (a) Conditions of radar subcarriers; (b) the power allocation results under $\mathcal{P}_{\max} = 10$ kW.

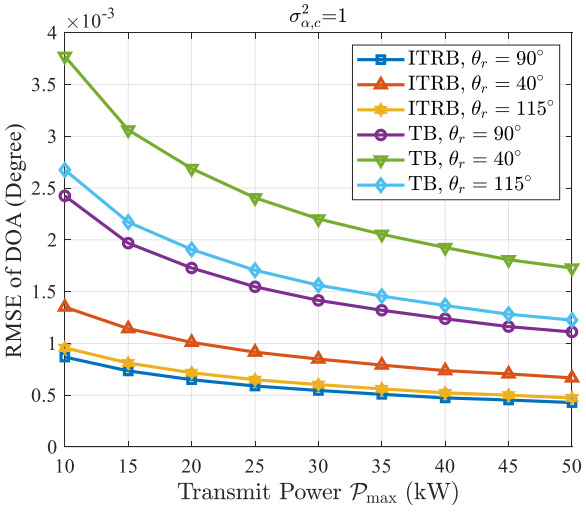

FIGURE 4. The RMSE of DOA estimation versus transmit power $\mathcal{P}_{\max}$ under $\sigma^2_{\alpha,c} = 1$.

technique achieves a better accuracy of TOA estimation compared with the TB technique.

Fig. 6 depicts the MMSE of localization estimation for different values of spatial angle θ_r and detection range d_r. Fig. 6(a) depicts the MMSE versus spatial angle under $\mathcal{P}_{\max} = 10$ kW and $d_r = 1$ kM. We can see that, as discussed

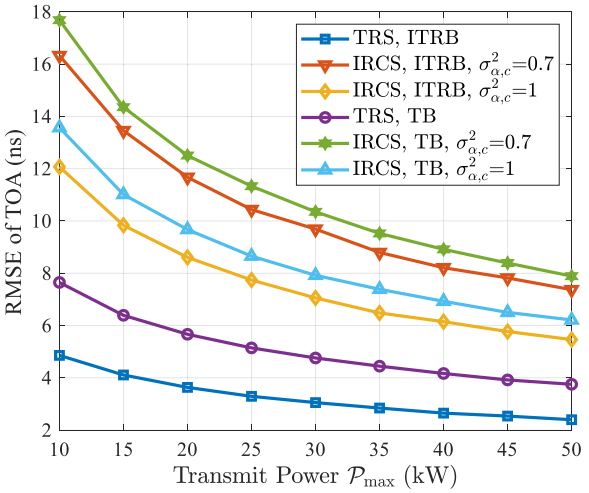

FIGURE 5. The RMSE of TOA estimation versus transmit power $\mathcal{P}_{\max}$.

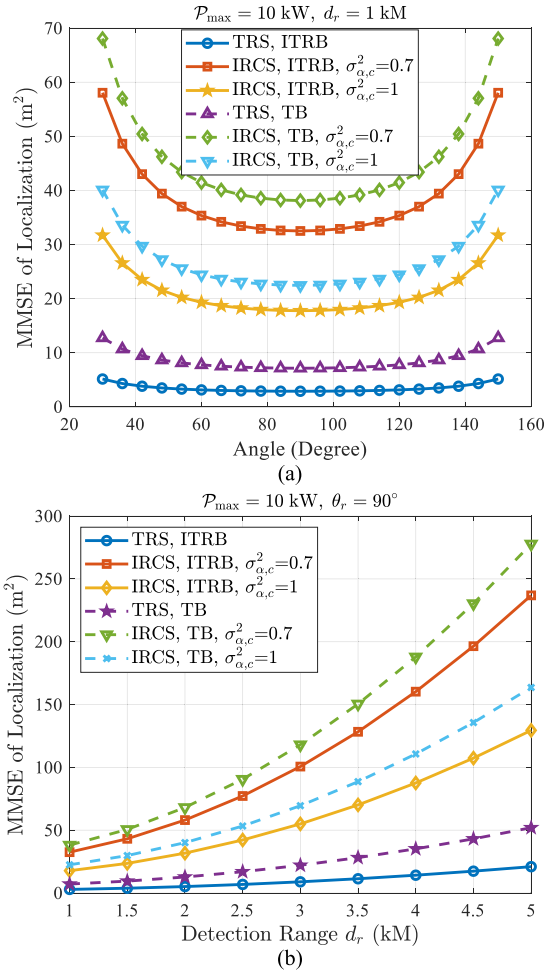

FIGURE 6. The MMSE of localization estimation for the IRCS and TRS. (a) The MMSE versus spatial angle under $\mathcal{P}_{\max} = 10$ kW and $d_r = 1$ kM; (b) the MMSE versus detection range d_r under $\mathcal{P}_{\max} = 10$ kW and $\theta_r = 90°$.

in section IV, the localization estimation is most accuracy when angle $\theta_r = 90°$ and the estimation accuracy is getting worse if θ_r is closing to 0° or 180°. Fig. 6(b) depicts the

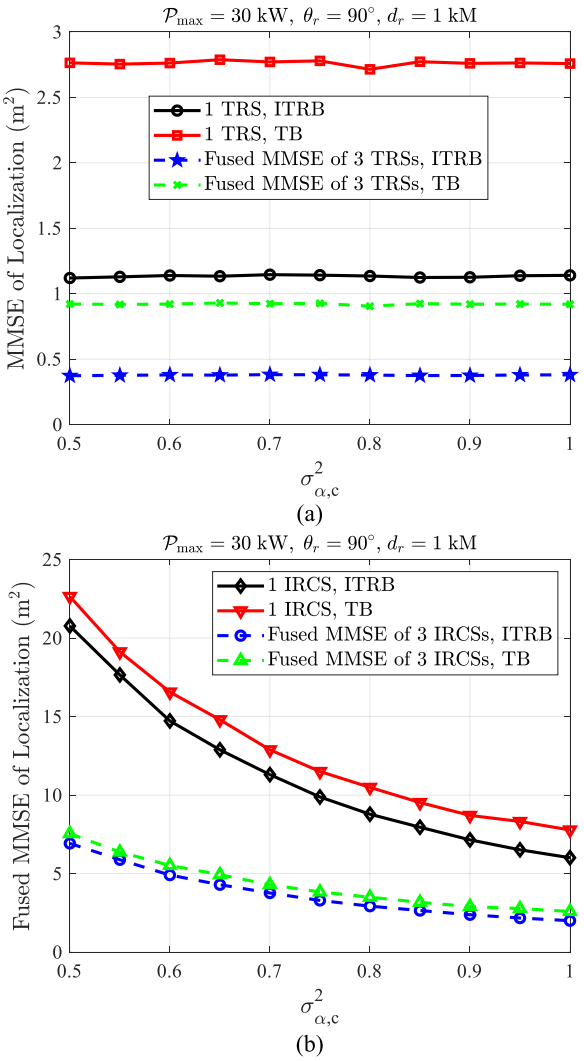

FIGURE 7. The MMSE of localization estimation versus variance $\sigma^2_{\alpha,c}$ under $\mathcal{P}_{\max} = 30$ kW, $\theta_r = 90°$ and $d_r = 1$ kM. a) For the TRS; b) for the IRCS.

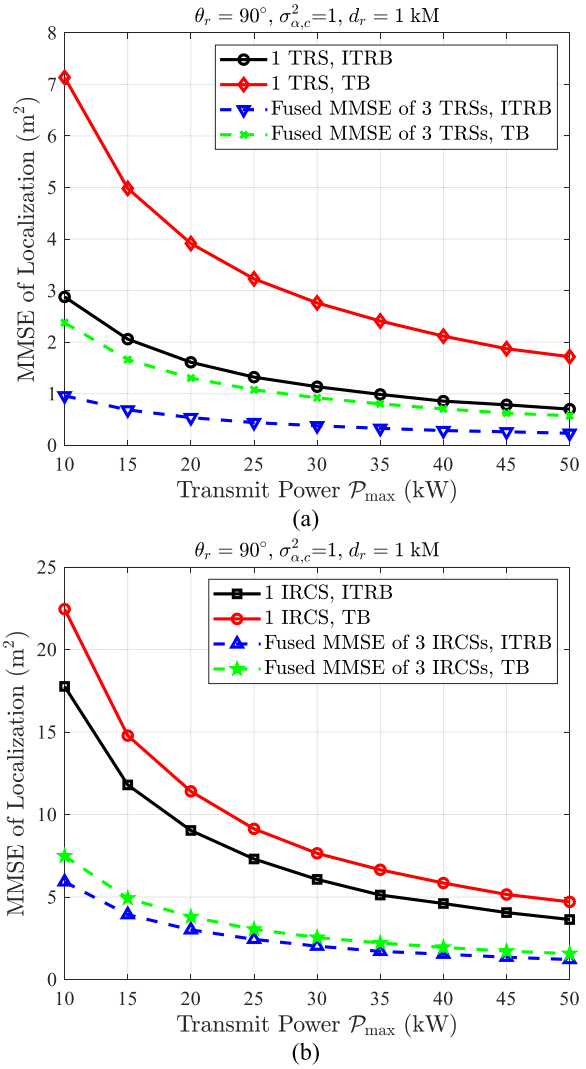

FIGURE 8. The MMSE of localization estimation versus transmit power $\mathcal{P}_{\max}$ under $\theta_r = 90°$, $\sigma^2_{\alpha,c} = 1$ and $d_r = 1$ kM. a) For the TRS; b) for the IRCS.

MMSE versus detection range d_r under $\mathcal{P}_{\max} = 10$ kW and $\theta_r = 90°$. We can see that, as expected, the larger detection range d_r is, the worse estimation accuracy is.

For both Fig. 6(a) and Fig. 6(b), comparing the cases of the IRCS and TRS, the MMSE for the IRCS is worse than that for the TRS, since the additional errors, i.e., the communication transmission error. We can also see that, for both IRCS and TRS, the ITRB technique achieves a better estimation accuracy, i.e., smaller MMSE, compared with the TB technique. Also, with larger variance $\sigma^2_{\alpha,c}$ (which implies better communication channel condition), the estimation accuracy is closing to the case of the TRS. To offer further insight, we look into the effect of different values of $\sigma^2_{\alpha,c}$ on the MMSE next.

Under $\mathcal{P}_{\max} = 30$ kW, $\theta_r = 90°$ and $d_r = 1$ kM, the MMSE of localization estimation versus variance $\sigma^2_{\alpha,c}$ for the TRS and IRCS are depicted in Fig. 7(a) and Fig. 7(b), respectively. In Fig. 7(a), we can see that, for the TRS, the estimation accuracy does not fluctuate with $\sigma^2_{\alpha,c}$, which is because only the radar estimation error is considered. The MMSE fused by $J = 3$ TRSs is much lower than the individual TRS, which means there is much benefit from linear fusion rule. In Fig. 7(b), we can see that, for the IRCS, the larger $\sigma^2_{\alpha,c}$ is, the better estimation accuracy is. The MMSE fused by $J = 3$ IRCSs is much lower than the individual IRCS. Further, the difference between the fused and individual MMSEs is getting smaller with larger $\sigma^2_{\alpha,c}$, which means there is much better fusion benefit for the larger $\sigma^2_{\alpha,c}$. Also, for the cases of both individual and fused MMSE depicted in Fig. 7(a) and Fig. 7(b), the ITRB technique achieves a better estimation accuracy compared with the TB technique.

Under $\theta_r = 90°$, $\sigma^2_{\alpha,c} = 1$ and $d_r = 1$ kM, the MMSEs of localization estimation versus the transmit power $\mathcal{P}_{\max}$ for

the TRS and IRCS are depicted in Fig. 8(a) and Fig. 8(b), respectively. We can see that, as expected, the (fused) MMSEs are smaller, i.e., better estimation accuracy, with larger transmit power $\mathcal{P}_{\max}$. The MMSE fused by $J = 3$ IRCSs (TRSs) is much lower than the individual IRCS (TRS). Further, the difference between the fused and individual MMSEs is getting smaller with larger $\mathcal{P}_{\max}$. Also, under a certain transmit power, the ITRB technique can improve the estimation accuracy for both TRS and IRCS. By comparing Fig. 8(a) and Fig. 8(b), it is seen that, under a certain transmit power $\mathcal{P}_{\max}$, the MMSE for the IRCS is worse than that for the TRS, since the additional errors, i.e., the communication transmission error.

VI. CONCLUSION

In this paper, exploiting multicarrier waveforms, the CRB of localization estimation for the IRCS network has been investigated. The functions of radar and communication are executed simultaneously by one multicarrier waveform. Firstly, the CRBs of TOA and DOA estimation have been derived for an individual IRCS. Under a certain transmit power, the transmit and receive beamformers of radar are iteratively optimized to maximize the radar SINR. Then, the CRB of localization estimation has been derived using hybrid TOA/DOA measurement. The local CRBs of the localization estimation from different IRCSs are fused according to the linear fusion rule at the FC. Finally, numerical results have demonstrated that the additional errors for the IRCS, i.e., the communication transmission error, are mainly determined by the channel conditions of communication and available transmit power; the estimation accuracy for both the IRCS and TRS can be improved through the ITRB technique.

A viable future work direction is to derive the stochastic CRB [39], [40] of localization estimation for the IRCS.

APPENDIX A
PROOF OF PROPOSITION 1

Define $\zeta_{1,j}, \cdots, \zeta_{K,j}$ as the eigenvalues of the positive semidefinite matrix $\boldsymbol{D}_j^{-1/2}\boldsymbol{\Phi}_j\boldsymbol{\Sigma}_{c,j}\boldsymbol{\Phi}_j^{\dagger}\boldsymbol{D}_j^{-1/2}$; then, for the case of large frequency spacing Δf, we have

$$\begin{aligned}
&\zeta_{k,j}\\
&= \sigma_{\alpha,c,k,j}^2\left|\boldsymbol{w}_{k,j}^{\dagger}\boldsymbol{A}\left(\theta_{c,j}\right)\boldsymbol{u}_{k,j}\right|^2 G_{k,j}^2\sigma_{\alpha,r,k,j}^2\eta_{k,j}\\
&\quad\times\Big[\sigma_{\boldsymbol{n},c,k}^2\left|\boldsymbol{w}_{k,j}^{\dagger}\boldsymbol{A}\left(\theta_{c,j}\right)\boldsymbol{u}_{k,j}\right|^2\\
&\quad\times G_{k,j}^2\left(\sigma_{I,k,\tilde{j}}^2\tilde{\eta}_{k,j}+\sigma_{n,r,k,j}^2\boldsymbol{v}_{k,j}^{\dagger}\boldsymbol{v}_{k,j}\right)+\sigma_{n,c,k}^2\boldsymbol{w}_{k,j}^{\dagger}\boldsymbol{w}_{k,j}\Big]^{-1}\\
&= \sigma_{\alpha,c,k,j}^2\left|\boldsymbol{w}_{k,j}^{\dagger}\boldsymbol{A}\left(\theta_{c,j}\right)\boldsymbol{u}_{k,j}\right|^2\sigma_{\alpha,r,k,j}^2\eta_{k,j}\left|s_{k,j}\right|^2\Big[\sigma_{\alpha,c,k,j}^2\\
&\quad\times\left|\boldsymbol{w}_{k,j}^{\dagger}\boldsymbol{A}\left(\theta_{c,j}\right)\boldsymbol{u}_{k,j}\right|^2\left|s_{k,j}\right|^2\left(\sigma_{I,k,\tilde{j}}^2\tilde{\eta}_{k,j}+\sigma_{n,r,k,j}^2\boldsymbol{v}_{k,j}^{\dagger}\boldsymbol{v}_{k,j}\right)\\
&\quad+\left(\sigma_{\alpha,r,k,j}^2\eta_j+\sigma_{I,k,\tilde{j}}^2\tilde{\eta}_j+\sigma_{n,r,k,j}^2\boldsymbol{v}_{k,j}^{\dagger}\boldsymbol{v}_{k,j}\right)\sigma_{n,c,k}^2\boldsymbol{w}_{k,j}^{\dagger}\boldsymbol{w}_{k,j}\Big]^{-1},
\end{aligned}\tag{49}$$

where $\eta_{k,j}$ and $\tilde{\eta}_{k,j}$ are given in Eqs. (7) and (8), respectively. Combining Eqs. (20) and (21), $\zeta_{k,j}$ can be further given by

$$\begin{aligned}
\zeta_{k,j} &= \Gamma_{c,k,j}\sigma_{\alpha,r,k,j}^2\eta_{k,j}\Big[\Gamma_{c,k,j}\left(\sigma_{I,k,\tilde{j}}^2\tilde{\eta}_j+\sigma_{n,r,k,j}^2\boldsymbol{v}_{k,j}^{\dagger}\boldsymbol{v}_{k,j}\right)\\
&\quad+\left(\sigma_{\alpha,r,k,j}^2\eta_j+\sigma_{I,k,\tilde{j}}^2\tilde{\eta}_{k,j}+\sigma_{\boldsymbol{n},r,k,j}^2\boldsymbol{v}_{k,j}^{\dagger}\boldsymbol{v}_{k,j}\right)\Big]^{-1}\\
&= \Gamma_{c,k,j}\Gamma_{r,k,j}\left(\Gamma_{c,k,j}+\Gamma_{r,k,j}+1\right)^{-1}.
\end{aligned}\tag{50}$$

Therefore, substitute Eq. (50) into Eq. (15), the CRBs of TOA estimation, i.e., $\mathcal{C}_{\tau,j,R+C}$, can be given by

$$\begin{aligned}
\mathcal{C}_{\tau,j,R+C} &= \frac{6\sum_{k=1}^{K}\zeta_{k,j}}{N_R\left(K\Delta f\right)^2}\\
&= \sum_{k=1}^{K}\frac{6\left(\Gamma_{c,k,j}\Gamma_{r,k,j}\left(\Gamma_{c,k,j}+\Gamma_{r,k,j}+1\right)^{-1}\right)}{N_R\left(K\Delta f\right)^2}\\
&= \sum_{k=1}^{K}\frac{6\left(\Gamma_{c,k,j}^{-1}+\Gamma_{r,k,j}^{-1}\left(1+\Gamma_{c,k,j}^{-1}\right)\right)}{N_R\left(K\Delta f\right)^2}.
\end{aligned}\tag{51}$$

Similarly, substitute Eq. (50) into Eq. (16), the CRBs of TOA estimation, i.e., $\mathcal{C}_{\theta,j,R+C}$, can be given by

$$\begin{aligned}
\mathcal{C}_{\theta,j,R+C} &= \frac{3\sum_{k=1}^{K}\zeta_{k,j}}{\pi^2\sin^2\theta_{r,j}N_R\left(N_R-1\right)\left(N_R+1\right)}\\
&= \sum_{k=1}^{K}\frac{\Gamma_{c,k,j}\Gamma_{r,k,j}\left(\Gamma_{c,k,j}+\Gamma_{r,k,j}+1\right)^{-1}}{\pi^2\sin^2\theta_{r,j}N_R\left(N_R-1\right)\left(N_R+1\right)}\\
&= \sum_{k=1}^{K}\frac{3\left(\Gamma_{c,k,j}^{-1}+\Gamma_{r,k,j}^{-1}\left(1+\Gamma_{c,k,j}^{-1}\right)\right)}{\pi^2\sin^2\theta_{r,j}N_R\left(N_R-1\right)\left(N_R+1\right)}.
\end{aligned}\tag{52}$$

APPENDIX B
ESTIMATION PERFORMANCE FOR TRS

Here, as a contrast, we present the estimation performance for the TRS. For the observed radar signal presented in (3), in view of the AWGN, the pdf of $\boldsymbol{y}_{r,j}$ conditioned on τ and θ is

$$p\left(\boldsymbol{y}_{r,j};\tau,\theta\right)=\frac{\exp\left(-\boldsymbol{y}_{r,j}{}^{\dagger}\left(\boldsymbol{H}_j\boldsymbol{\Sigma}_{r,j}\boldsymbol{H}_j^{\dagger}+\boldsymbol{C}\right)^{-1}\boldsymbol{y}_{r,j}\right)}{\pi^K\det\left(\boldsymbol{H}_j\boldsymbol{\Sigma}_{r,j}\boldsymbol{H}_j^{\dagger}+\boldsymbol{C}\right)},\tag{53}$$

where

$$\boldsymbol{C}=\sum_{\tilde{j}=1,\tilde{j}\neq j}^{J}\boldsymbol{H}_{I,\tilde{j}}\boldsymbol{\Sigma}_{I,\tilde{j}}\boldsymbol{H}_{I,\tilde{j}}^{\dagger}+\boldsymbol{V}_j\boldsymbol{V}_j^{\dagger}\tag{54}$$

is the interference-plus-noise covariance matrix. The TOA/DOA ML estimation can be found by jointly searching over (τ_j, θ_j) to maximize $p\left(\boldsymbol{y}_{r,j};\tau,\theta\right)$. The joint ML estimator is unbiased and the CRB for (τ_j, θ_j) is a function of the SNR [42]–[45]. Then, the CRBs of TOA and DOA estimation, i.e., $\mathcal{C}_{\tau,j,R}$ and $\mathcal{C}_{\theta,j,R}$, for the TRS can be given by [27]

$$\mathcal{C}_{\tau,j,R}=\frac{6tr\left(\boldsymbol{C}^{-1/2}\boldsymbol{H}_j\boldsymbol{\Sigma}_{r,j}\boldsymbol{H}_j^{\dagger}\boldsymbol{C}^{-1/2}\right)^{-1}}{N_R\left(K\Delta f\right)^2},\tag{55}$$

$$\mathcal{C}_{\theta,j,R} = \frac{3tr\left(\boldsymbol{C}^{-1/2}\boldsymbol{H}_j\boldsymbol{\Sigma}_{r,j}\boldsymbol{H}_j^{\dagger}\boldsymbol{C}^{-1/2}\right)^{-1}}{\pi^2\sin^2\theta_{r,j}N_R\left(N_R-1\right)\left(N_R+1\right)}, \tag{56}$$

respectively.

Define $\xi_{r,1,j}, \cdots, \xi_{r,K,j}$ as the eigenvalues of the positive semidefinite matrix $\boldsymbol{C}^{-1/2}\boldsymbol{H}_j\boldsymbol{\Sigma}_{r,j}\boldsymbol{H}_j^{\dagger}\boldsymbol{C}^{-1/2}$. Since frequency spacing among the subcarriers is sufficiently large, $\xi_{r,k,j} = \Gamma_{r,k,j}$. Therefore, the CRBs of TOA and DOA estimation, i.e., $\mathcal{C}_{\tau,j,R}$ and $\mathcal{C}_{\theta,j,R}$, for the TRS can be, respectively, written as

$$\begin{aligned}\mathcal{C}_{\tau,j,R} &= \frac{6\sum_{k=1}^{K}\xi_{r,k,j}^{-1}}{N_R\left(K\Delta f\right)^2} \\ &= \frac{6\sum_{k=1}^{K}\Gamma_{r,k,j}^{-1}}{N_R\left(K\Delta f\right)^2},\end{aligned} \tag{57}$$

$$\begin{aligned}\mathcal{C}_{\theta,j,R} &= \frac{3\sum_{k=1}^{K}\xi_{r,k,j}^{-1}}{\pi^2\sin^2\theta_{r,j}N_R\left(N_R-1\right)\left(N_R+1\right)} \\ &= \frac{3\sum_{k=1}^{K}\Gamma_{r,k,j}^{-1}}{\pi^2\sin^2\theta_{r,j}N_R\left(N_R-1\right)\left(N_R+1\right)}.\end{aligned} \tag{58}$$

Similar to the way of deriving the CRB of localization estimation for the IRCS (which is depicted in Eq. (45)), the CRB of localization estimation for the TRS, i.e., $\mathcal{C}_{\boldsymbol{p}_T,j,R}$, can be given by

$$\mathcal{C}_{\boldsymbol{p}_T,j,R} = d_{r,j}^2\mathcal{C}_{\theta,j,R} + c^2\mathcal{C}_{\tau,j,R}. \tag{59}$$

Further, the fused CRB of localization estimation for the TRS, i.e., $\mathcal{C}_{\boldsymbol{p}_T,R}^{glo}$, can be given by

$$\mathcal{C}_{\boldsymbol{p}_T,R}^{glo} = \left(\sum_{j=1}^{J}\left(d_{r,j}^2\mathcal{C}_{\theta,j,R} + c^2\mathcal{C}_{\tau,j,R}\right)^{-1}\right)^{-1}. \tag{60}$$

REFERENCES

[1] A. Hassanien, M. G. Amin, E. Aboutanios, and B. Himed, "Dual-function radar communication systems: A solution to the spectrum congestion problem," *IEEE Signal Process. Mag.*, vol. 36, no. 5, pp. 115–126, Sep. 2019.
[2] X. Li, Z. Sun, W. Yi, G. Cui, L. Kong, and X. Yang, "Computationally efficient coherent detection and parameter estimation algorithm for maneuvering target," *Signal Process.*, vol. 155, pp. 130–142, Feb. 2019.
[3] X. Li, D. Wang, W.-Q. Wang, W. Liu, and X. Ma, "Range-angle localization of targets with planar frequency diverse subaperturing MIMO radar," *IEEE Access*, vol. 6, pp. 12505–12517, Mar. 2018.
[4] X. Du, A. Aubry, A. De Maio, and G. Cui, "Toeplitz structured covariance matrix estimation for radar applications," *IEEE Signal Process. Lett.*, vol. 27, pp. 595–599, Apr. 2020.
[5] H. Gao, S. Zhang, Y. Su, and M. Diao, "Joint resource allocation and power control algorithm for cooperative D2D heterogeneous networks," *IEEE Access*, vol. 7, pp. 20632–20643, Jan. 2019.
[6] L. Zheng, M. Lops, Y. C. Eldar, and X. Wang, "Radar and communication coexistence: An overview: A review of recent methods," *IEEE Signal Process. Mag.*, vol. 36, no. 5, pp. 85–99, Sep. 2019.
[7] T. Song, Y. Wang, G. Li, and S. Pang, "Server consolidation energy-saving algorithm based on resource reservation and resource allocation strategy," *IEEE Access*, vol. 7, pp. 171452–171460, Nov. 2019.
[8] T. Tian, T. Zhang, and L. Kong, "Timeliness constrained task scheduling for multifunction radar network," *IEEE Sensors J.*, vol. 19, no. 2, pp. 525–534, Jan. 2019.
[9] A. R. Chiriyath, B. Paul, G. M. Jacyna, and D. W. Bliss, "Inner bounds on performance of radar and communications co-existence," *IEEE Trans. Signal Process.*, vol. 64, no. 2, pp. 464–474, Jan. 2016.
[10] A. Khawar, A. Abdelhadi, and C. Clancy, "Target detection performance of spectrum sharing MIMO radars," *IEEE Sensors J.*, vol. 15, no. 9, pp. 4928–4940, Sep. 2015.
[11] L. Zheng, M. Lops, X. Wang, and E. Grossi, "Joint design of overlaid communication systems and pulsed radars," *IEEE Trans. Signal Process.*, vol. 66, no. 1, pp. 139–154, Jan. 2018.
[12] K. Singh, S. Biswas, T. Ratnarajah, and F. A. Khan, "Transceiver design and power allocation for full-duplex MIMO communication systems with spectrum sharing radar," *IEEE Trans. Cognit. Commun. Netw.*, vol. 4, no. 3, pp. 556–566, Sep. 2018.
[13] Y. L. Sit, B. Nuss, and T. Zwick, "On mutual interference cancellation in a MIMO OFDM multiuser radar-communication network," *IEEE Trans. Veh. Technol.*, vol. 67, no. 4, pp. 3339–3348, Apr. 2018.
[14] C. Shi, F. Wang, M. Sellathurai, J. Zhou, and S. Salous, "Power minimization-based robust OFDM radar waveform design for radar and communication systems in coexistence," *IEEE Trans. Signal Process.*, vol. 66, no. 5, pp. 1316–1330, Mar. 2018.
[15] C. Shi, F. Wang, S. Salous, and J. Zhou, "Low probability of intercept-based optimal OFDM waveform design strategy for an integrated radar and communications system," *IEEE Access*, vol. 6, pp. 57689–57699, Oct. 2018.
[16] B. Li, A. P. Petropulu, and W. Trappe, "Optimum co-design for spectrum sharing between matrix completion based MIMO radars and a MIMO communication system," *IEEE Trans. Signal Process.*, vol. 64, no. 17, pp. 4562–4575, Sep. 2016.
[17] T. Tian, T. Zhang, G. Li, and T. Zhou, "Mutual information-based power allocation and co-design for multicarrier radar and communication systems in coexistence," *IEEE Access*, vol. 7, pp. 159300–159312, Nov. 2019.
[18] F. Wang, H. Li, and M. A. Govoni, "Power allocation and co-design of multicarrier communication and radar systems for spectral coexistence," *IEEE Trans. Signal Process.*, vol. 67, no. 14, pp. 3818–3831, Jul. 2019.
[19] S. D. Blunt, M. R. Cook, and J. Stiles, "Embedding information into radar emissions via waveform implementation," in *Proc. Int. Waveform Diversity Design Conf.*, Niagara Falls, ON, Canada, Aug. 2010, pp. 195–199.
[20] A. Hassanien, M. G. Amin, Y. D. Zhang, and F. Ahmad, "Signaling strategies for dual-function radar communications: An overview," *IEEE Aerosp. Electron. Syst. Mag.*, vol. 31, no. 10, pp. 36–45, Oct. 2016.
[21] J. Euziere, R. Guinvarc'h, M. Lesturgie, B. Uguen, and R. Gillard, "Dual function radar communication time-modulated array," in *Proc. Int. Radar Conf.*, Lille, France, 2014, pp. 1–4.
[22] A. Hassanien, M. G. Amin, Y. D. Zhang, and F. Ahmad, "Dual-function radar-communications: Information embedding using sidelobe control and waveform diversity," *IEEE Trans. Signal Process.*, vol. 64, no. 8, pp. 2168–2181, Apr. 2016.
[23] A. Hassanien, M. G. Amin, Y. D. Zhang, and F. Ahmad, "Dual-function radar-communications using phase-rotational invariance," in *Proc. 23rd Eur. Signal Process. Conf. (EUSIPCO)*, Nice, France, Aug. 2015, pp. 1346–1350.
[24] A. Hassanien, M. G. Amin, Y. D. Zhang, F. Ahmad, and B. Himed, "Non-coherent PSK-based dual-function radar-communication systems," in *Proc. IEEE Radar Conf. (RadarConf)*, Philadelphia, PA, USA, May 2016, pp. 1–6.
[25] A. Hassanien, M. G. Amin, Y. D. Zhang, and F. Ahmad, "Phase-modulation based dual-function radar-communications," *IET Radar, Sonar Navigat.*, vol. 10, no. 8, pp. 1411–1421, Oct. 2016.
[26] A. Ahmed, Y. D. Zhang, and Y. Gu, "Dual-function radar-communications using QAM-based sidelobe modulation," *Digit. Signal Process.*, vol. 82, pp. 166–174, Nov. 2018.
[27] S. M. Kay, *Fundamentals of Statistical Signal Processing*. Upper Saddle River, NJ, USA: Prentice-Hall, 1993.
[28] N. Patwari, J. N. Ash, S. Kyperountas, A. O. Hero, R. L. Moses, and N. S. Correal, "Locating the nodes: Cooperative localization in wireless sensor networks," *IEEE Signal Process. Mag.*, vol. 22, no. 4, pp. 54–69, Jul. 2005.
[29] Z.-M. Liu, Z.-T. Huang, and Y.-Y. Zhou, "Direction-of-arrival estimation of wideband signals via covariance matrix sparse representation," *IEEE Trans. Signal Process.*, vol. 59, no. 9, pp. 4256–4270, Sep. 2011.
[30] Q. Shen, W. Liu, W. Cui, S. Wu, Y. D. Zhang, and M. G. Amin, "Low-complexity direction-of-arrival estimation based on wideband co-prime arrays," *IEEE/ACM Trans. Audio, Speech, Language Process.*, vol. 23, no. 9, pp. 1445–1456, Sep. 2015.
[31] Q. Shen, W. Liu, W. Cui, and S. Wu, "Underdetermined DOA estimation under the compressive sensing framework: A review," *IEEE Access*, vol. 4, pp. 8865–8878, Jan. 2016.

[32] M. S. Greco, P. Stinco, F. Gini, and A. Farina, "Cramer–Rao bounds and selection of bistatic channels for multistatic radar systems," *IEEE Trans. Aerosp. Electron. Syst.*, vol. 47, no. 4, pp. 2934–2948, Oct. 2011.
[33] S. Choi, J. Chun, I. Paek, and J. Jang, "A stochastic CRB for non-unitary beam-space transformations and its application to optimal steering angle design," *IEEE Signal Process. Lett.*, vol. 22, no. 11, pp. 2014–2018, Nov. 2015.
[34] I. Bekkerman and J. Tabrikian, "Target detection and localization using MIMO radars and sonars," *IEEE Trans. Signal Process.*, vol. 54, no. 10, pp. 3873–3883, Oct. 2006.
[35] F. Wen, "Computationally efficient DOA estimation algorithm for MIMO radar with imperfect waveforms," *IEEE Commun. Lett.*, vol. 23, no. 6, pp. 1037–1040, Jun. 2019.
[36] H. Yu, X. Qiu, X. Zhang, C. Wang, and G. Yang, "Two-dimensional direction of arrival (DOA) estimation for rectangular array via compressive sensing trilinear model," *Int. J. Antennas Propag.*, vol. 2015, May 2015, Art. no. 297572.
[37] H. Chen, C. Hou, W. Liu, W.-P. Zhu, and M. N. S. Swamy, "Efficient two-dimensional direction-of-arrival estimation for a mixture of circular and noncircular sources," *IEEE Sensors J.*, vol. 16, no. 8, pp. 2527–2536, Apr. 2016.
[38] F. Wen, J. Shi, and Z. Zhang, "Joint 2D-DOD, 2D-DOA, and polarization angles estimation for bistatic EMVS-MIMO radar via PARAFAC analysis," *IEEE Trans. Veh. Technol.*, vol. 69, no. 2, pp. 1626–1638, Feb. 2020.
[39] F. Wen, J. Shi, and Z. Zhang, "Direction finding for bistatic MIMO radar with unknown spatially colored noise," *Circuits, Syst., Signal Process.*, vol. 39, no. 5, pp. 2412–2424, May 2020.
[40] F. Wen, X. Zhang, and Z. Zhang, "CRBs for direction-of-departure and direction-of-arrival estimation in collocated MIMO radar in the presence of unknown spatially coloured noise," *IET Radar, Sonar Navigat.*, vol. 13, no. 4, pp. 530–537, Apr. 2019.
[41] Q. He and R. S. Blum, "Cramer–Rao bound for MIMO radar target localization with phase errors," *IEEE Signal Process. Lett.*, vol. 17, no. 1, pp. 83–86, Jan. 2010.
[42] M. Wax and A. Leshem, "Joint estimation of time delays and directions of arrival of multiple reflections of a known signal," *IEEE Trans. Signal Process.*, vol. 45, no. 10, pp. 2477–2484, Oct. 1997.
[43] Y. Fu and Z. Tian, "Cramer–Rao bounds for hybrid TOA/DOA-based location estimation in sensor networks," *IEEE Signal Process. Lett.*, vol. 16, no. 8, pp. 655–658, Aug. 2009.
[44] W. Meng, W. Xiao, and L. Xie, "Distributed algorithm for hybrid TOA/DOA-based source localization," in *Proc. 6th IEEE Conf. Ind. Electron. Appl.*, Jun. 2011, pp. 1046–1049.
[45] C. de Moustier, "Time and angle of arrival uncertainties in echo-sounding," in *Proc. IEEE-Spain OCEANS*, Jun. 2011, pp. 1–5.
[46] K. M. Rabie and B. Adebisi, "Enhanced amplify-and-forward relaying in non-Gaussian PLC networks," *IEEE Access*, vol. 5, pp. 4087–4094, Mar. 2017.
[47] I. Krikidis, J. Thompson, S. Mclaughlin, and N. Goertz, "Amplify-and-forward with partial relay selection," *IEEE Commun. Lett.*, vol. 12, no. 4, pp. 235–237, Apr. 2008.
[48] Y. Yang and R. Blum, "MIMO radar waveform design based on mutual information and minimum mean-square error estimation," *IEEE Trans. Aerosp. Electron. Syst.*, vol. 43, no. 1, pp. 330–343, Jan. 2007.
[49] H. S. Simon, *Adaptive Filter Theory*. Noida, India: Pearson, 2008.
[50] R. A. Romero, J. Bae, and N. A. Goodman, "Theory and application of SNR and mutual information matched illumination waveforms," *IEEE Trans. Aerosp. Electron. Syst.*, vol. 47, no. 2, pp. 912–927, Apr. 2011.
[51] B. Tang and J. Li, "Spectrally constrained MIMO radar waveform design based on mutual information," *IEEE Trans. Signal Process.*, vol. 67, no. 3, pp. 821–834, Feb. 2019.
[52] H. Li and B. Himed, "Transmit subaperturing for MIMO radars with co-located antennas," *IEEE J. Sel. Topics Signal Process.*, vol. 4, no. 1, pp. 55–65, Feb. 2010.
[53] J. Liu, H. Li, and B. Himed, "Joint optimization of transmit and receive beamforming in active arrays," *IEEE Signal Process. Lett.*, vol. 21, no. 1, pp. 39–42, Jan. 2014.
[54] M. Skolnik, *Radar Handbook*, 3rd ed. New York, NY, USA: McGraw-Hill, 2008.
[55] M. Grant and S. Boyd. (Feb. 2012). *CVX Package*. [Online]. Available: http://www.cvxr.com/cvx.r
[56] A. Aubry, A. DeMaio, A. Farina, and M. Wicks, "Knowledge-aided (potentially cognitive) transmit signal and receive filter design in signal-dependent clutter," *IEEE Trans. Aerosp. Electron. Syst.*, vol. 49, no. 1, pp. 93–117, Jan. 2013.
[57] Y. Fu, Q. Ling, and Z. Tian, "Distributed sensor allocation for multi-target tracking in wireless sensor networks," *IEEE Trans. Aerosp. Electron. Syst.*, vol. 48, no. 4, pp. 3538–3553, Oct. 2012.
[58] E. Waltz and J. Llinas, *Multisensor Data Fusion*. Boston, MA, USA: Artech House, 1990.

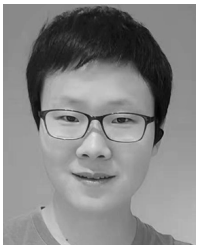

TUANWEI TIAN is currently pursuing the Ph.D. degree with the School of Information and Communication Engineering, University of Electronic Science and Technology of China, Chengdu, China. Since April 2019, he has been a Visiting Student Researcher with the Department of Electrical Engineering and Information Technologies, University of Naples Federico II, Napoli, Italy. His research interests include radar/communication co-existence, resource optimization, and radar task scheduling.

XIAOLIN DU was born in Tai'an, Shandong, China, in 1985. He received the B.S. and M.S. degrees from the Taiyuan University of Technology, Taiyuan, in 2008 and 2011, respectively, and the Ph.D. degree from Xidian University, Xi'an, in 2015. Since 2016, he has been a Faculty Member with the School of Computer and Control Engineering, Yantai University, Yantai, China. From 2019 to 2020, he was a Visiting Scholar with the Department of Electrical Engineering and Information Technology, University of Naples Federico II, Italy. His research interests include radar signal processing and waveform optimization.

GUCHONG LI (Student Member, IEEE) received the B.S. degree in electrical engineering from the University of Electronic Science and Technology of China (UESTC), China, in 2016, where he is currently pursuing the Ph.D. degree. He is also a Visiting Student with the Dipartimento di Ingegneria dell'Informazione, Università degli Studi di Firenze, Firenze, Italy. His current research interests include random finite set, target tracking, and data fusion.